ACS Photonics

Letter

Cite This: ACS Photonics 2018, 5, 3513−3518

pubs.acs.org/journal/apchd5

Smith−Purcell Radiation from Low-Energy Electrons

Aviram Massuda,*[,†,‡] Charles Roques-Carmes,[†,‡] Yujia Yang,[‡] Steven E. Kooi,[§] Yi Yang,[†,‡] Chitraang Murdia,[†] Karl K. Berggren,[‡] Ido Kaminer,[†,∥] and Marin Soljačić[†]

[†]Department of Physics, Massachusetts Institute of Technology, 77 Massachusetts Avenue, Cambridge, Massachusetts 02139, United States

[‡]Department of Electrical Engineering and Computer Science, Massachusetts Institute of Technology, 50 Vassar Street, Cambridge, Massachusetts 02139, United States

[§]Institute for Soldier Nanotechnologies, 77 Massachusetts Avenue, Cambridge, Massachusetts 02139, United States

[∥]Department of Electrical Engineering and Solid State Institute, Technion−Israel Institute of Technology, 32000 Haifa, Israel

Supporting Information

ABSTRACT: Recent advances in the fabrication of nanostructures and nanoscale features in metasurfaces offer new prospects for generating visible light emission from low-energy electrons. Here we present the experimental observation of visible light emission from low-energy free electrons interacting with nanoscale periodic surfaces through the Smith−Purcell (SP) effect. We demonstrate SP light emission from nanoscale gratings with periodicity as small as 50 nm, enabling the observation of tunable visible radiation from low-energy electrons (1.5 to 6 keV), an order of magnitude lower in energy than previously reported. We study the emission wavelength and intensity dependence on the grating pitch and electron energy, showing agreement between experiment and theory. Our results open the way to the production of SP-based nanophotonics integrated devices. Built inside electron microscopes, SP sources could enable the development of novel electron−optical correlated spectroscopic techniques and facilitate the observation of new quantum effects in light sources.

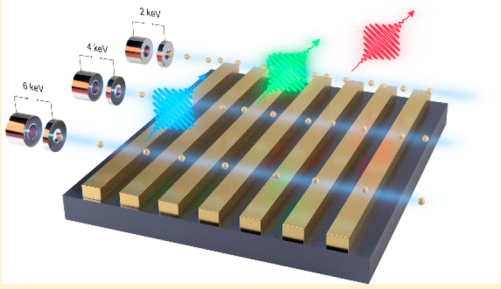

KEYWORDS: *light−matter interactions, periodic structures, nanophotonics, free-electron light sources*

Tunable nanoscale light sources are of the utmost importance for nanophotonics. Free-electron-driven light sources offer a promising avenue for achieving this goal.[1−5] These devices benefit from flexible material choices as well as from the ability to focus electrons to nanoscale spots, which in turn enables the tailoring of efficient interactions with nanoscale structures. Thus far, most free-electron radiation sources have used relativistic electrons ranging from highly relativistic energies as in synchrotrons and free electron lasers[6,7] to modestly relativistic energies as radiation sources in the microwave[6,8] and visible[1,9−12] regimes. The requirement for large electron velocities in those conventional setups has kept free-electron light sources away from compact or on-chip applications.

Recent advances in nanoscale fabrication techniques have enabled the study of new fundamental effects and their applications involving the interaction of free electrons with light and matter. For instance, new opportunities to explore the Smith−Purcell (SP) effect in nanoscale structures such as plasmonic arrays[13,14] and metasurfaces[15,16] have been recently investigated. Such systems can be used as sources of visible and infrared light that are tunable by adjusting the electron velocity.[9] The possibility of observing *shorter* wavelength emissions from relatively low-energy electrons (accessible with regular scanning or transmission electron microscopes, SEM or TEM) is a very promising field of research,[2,5,17−19] because of the exciting applications of short-wavelength radiation in beam diagnostics,[17] particle detection,[20] biological imaging in the water window,[21] and nanolithography.[22]

SP radiation is emitted when an electron passes in close proximity over a periodic surface, inducing charges at the surface of the grating to rearrange themselves to screen the field of the moving electron, thereby inducing the emission of electromagnetic radiation.[9,10] In 1953[9] Smith and Purcell measured the electromagnetic radiation produced by a free-electron beam passing over a metallic grating. They found that the radiated wavelength, λ, depends on the grating pitch, a, and the exciting electron velocity, $\beta = v/c$, where c is the speed of light, following the formula:

$$\lambda = \frac{a}{m}\left(\frac{1}{\beta} - \cos\theta\right) \tag{1}$$

where m is the diffraction order, $\beta = v/c$ is the normalized speed of an electron passing over the structure, and θ is the angle of emission measured from the direction of beam propagation.

Received: June 2, 2018
Published: August 30, 2018

DOI: 10.1021/acsphotonics.8b00743
ACS Photonics 2018, 5, 3513−3518

Smith and Purcell used relatively high-energy electrons with $\beta \approx 0.8$ for their original experiment. Further experimental demonstrations of the SP effect confirmed that it occurs over a wide spectral range. SP radiation has been demonstrated experimentally (or else proposed) in the visible,[2,9−12] far-infrared,[23] and THz and millimeter wave regimes.[24−26] Until now, these experimental demonstrations of SP radiation relied on the use of electrons that are moderately or highly relativistic, with the lowest electron energy to generate SP radiation being 12 keV.[14] In these experiments, relatively large-pitch periodic structures have been used to record SP radiation. The original experiment used metallic gratings of 1.67 μm pitch; in more recent experiments, the structure periodicity has been scaled down to 130 nm.[13] Reducing the periodicity to 50 nm enables us to observe optical SP radiation produced by nonrelativistic electron energies (about 5−10% the speed of light) and with an order of magnitude lower than the previous record.[14]

The key challenge in observing optical SP radiation from a nanograting is aligning the electron beam with a nanograting that is limited in size by nanofabrication constraints (typically about 200 μm along each lateral dimension parallel to the surface). We overcome this challenge by using a proprietary setup that we have developed. The setup makes it possible to spatially resolve the light emission while simultaneously collecting the emission spectra.[14] This way we can image the location of electron interaction with the surface and thus align the electron beam path with the nanograting and maximize the interaction between the two. Since the electron beam passing over the grating is incoherent, so is the resulting radiation.

We fabricated gold grating samples with 50 and 60 nm periods using electron beam lithography (EBL) and a lift-off technique (see Methods). The samples consist of gold lines on a thick gold layer over a 200 μm × 200 μm area. The samples were mounted inside the chamber of a modified SEM experimental setup (Figure 2), and the electron kinetic energy was tuned between 1.5 and 6 keV.

Figure 3a shows the measured SP spectra from a 50 nm pitch gold grating sample, with the peaks compared to the theoretical prediction (eq 1) down to an electron energy of 1.5 keV. In addition to the tunable SP peaks, the spectra show a strong cathodoluminescence (CL) background around 550 nm.

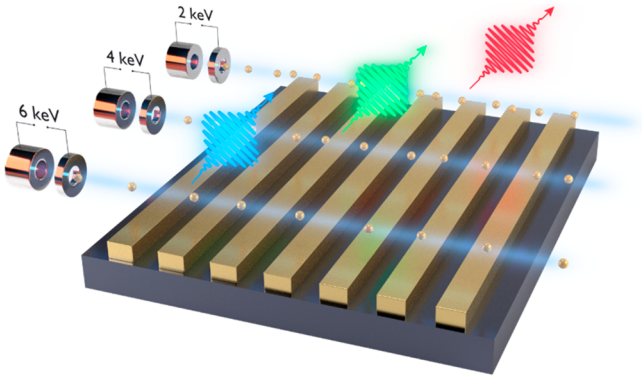

Figure 1. Observation of visible SP radiation from low-energy electrons. Sketch of the physics of our experiment: SP radiation is emitted when electrons pass in close proximity to a periodic structure. Varying the electron kinetic energy enables tunability of the SP radiation wavelength.

Figure 4a shows the measured SP spectra from 60 nm pitch gold nanogratings (shown in Figure 4b), with the peaks compared to the theoretical prediction (eq 1) at electron energies of 2−6 keV. Using power calibration measurements (see Methods), we estimate power levels on the order of ∼100 pW with a beam current of 100 nA (see Methods).

In Figure 3a and Figure 4a, gold gratings of period a = 50 and 60 nm are shown to produce SP emission over the 395−654 nm wavelength range with low-energy electrons (1.5−6 keV). To the best of our knowledge, these periodicities and electron kinetic energies used to generate SP radiation are the smallest reported so far (by a factor of 2.6 in the pitch and 8 in the kinetic energy). Our experimental observations are confirmed by simulations (Figure 4c and d), which also predict the spectrum line shape and take into account the structure geometry and the optical response of the material. The simulation computes the scattering spectrum of the evanescent field carried by the electron and verifies the typical cosine-like shape of the original formula (eq 1) as shown in Figure 4c. Interestingly, due to the optical response of the nanograting at the optical frequencies, the most efficient wavelengths of emission are usually emitted at some backward angle ($\theta > \frac{\pi}{2}$) (see Figure 4d). This fact explains the slight red-shift between the theoretical prediction at normal emission (dashed lines) and the peak wavelength, as can be seen in both our experimental and simulation results (Figure 4a). However, the angle and spectral density of SP radiation can be readily engineered using aperiodic and chirped structures.[16,27]

An advantage of using slow electrons is their higher photon extraction efficiency, $\eta = \frac{\mathrm{d}N/\mathrm{d}\omega}{E_k}$, where $\mathrm{d}N/\mathrm{d}\omega$ is the radiation intensity (generated number of photons per frequency) and E_k is the kinetic energy of electrons. To exemplify this advantage, we compute these quantities for a fixed radiation wavelength of 700 nm (Figure 5a). The electron structure separation is taken to be the same as the pitch of the nanograting, and the radiation is calculated for one unit cell, so that the geometry is invariant by scaling with β. We have recently predicted that slower electrons radiate more strongly than relativistic ones if placed at subwavelength separation from structures.[30] Here in Figure 5, we show that for the far-field separations, the radiation intensity decreases for smaller electron velocities (blue curve in Figure 5a). However, the extraction *efficiency* (defined by the ratio between the number of emitted photons and the kinetic energy of the electrons) increases with smaller electron velocities (red curve in Figure 5a), which indicates that slow electrons can potentially give rise to radiators with higher overall efficiency. For example, the extraction efficiency for β = 0.1 is 1 order of magnitude higher than the extraction efficiency for β = 0.6.

Finally, we experimentally observe that the SP spectral peak at each fixed emission wavelength gets narrower for smaller electron velocities; that is, when fixing the emission wavelength, lower electron velocities give a narrower emission spectrum. Figure 5b depicts this effect by showing the SP radiation at a fixed wavelength (700 nm) from three different nanograting pitches with three different electron velocities. This is consistent with the SP formula (eq 1), as it implies that the spectral bandwidth of SP radiation is linear with the electron velocity. The relationship can be obtained by fixing the peak wavelength, $\lambda_{peak} = \frac{a}{m}\frac{1}{\beta}$, and the collection numerical aperture, and then noticing that eq 1 gives $\Delta\lambda \propto \frac{a}{m} = \beta\lambda_{peak}$.

DOI: 10.1021/acsphotonics.8b00743
ACS Photonics 2018, 5, 3513−3518

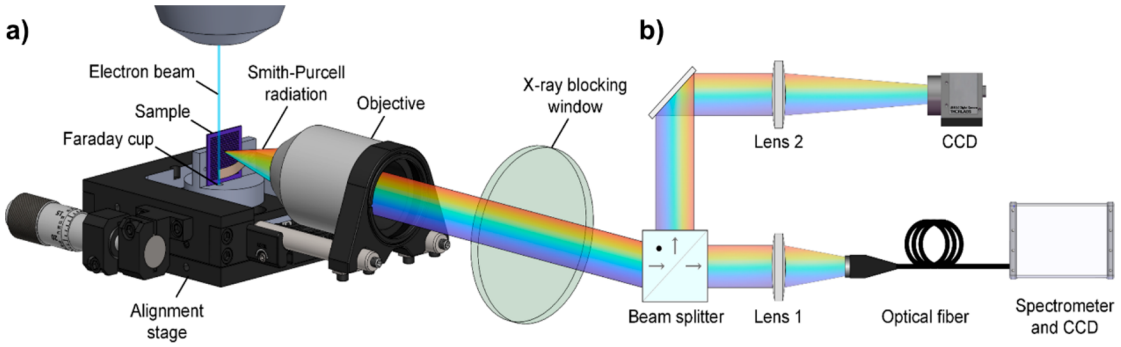

Figure 2. Illustration of our SEM-based experimental setup used to observe SP radiation. (a) Inside the SEM vacuum chamber the sample is held so that its surface is almost parallel to the path of the electron beam. The emitted light is collected by an objective and (b) directed to a beam splitter splitting the optical beam to an optical fiber collector that leads to a spectrometer (lens 1) and to a CCD camera (lens 2) that images the surface of the sample.

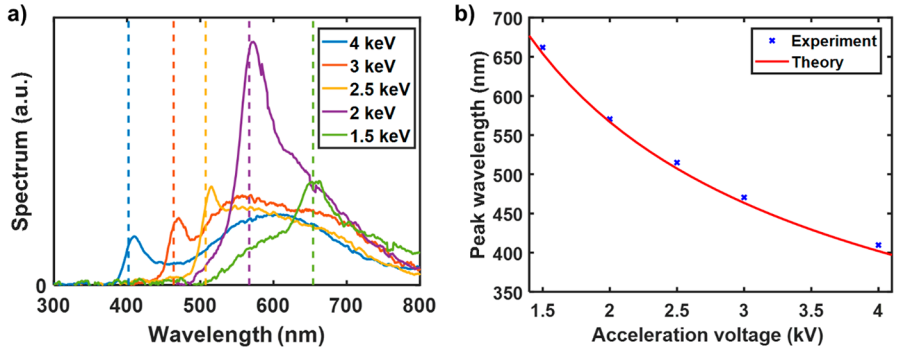

Figure 3. SP radiation from low electron velocities and small pitch grating. (a) Measured spectra for different kinetic energies from a grating with a 50 nm pitch. The dashed vertical lines are calculated according to the conventional SP theory at normal emission,[9] with colors corresponding to different kinetic energies. The spectra are normalized by the measured beam current. (b) Peak wavelength comparison between experiment and theory at normal emission[9] ($\theta = \pi/2$).

The effect of SP bandwidth narrowing for slow electrons also bolsters interest in observing SP radiation from even lower energy nonrelativistic electrons, yielding an additional degree of freedom to shape the spectral response of SP radiation.

In conclusion, while most of the literature has focused on moderately or highly relativistic electrons, the prospect of achieving a low-electron-energy nanoscale light source paves the way for new regimes of light−matter interaction. We developed a modified SEM that allows us to resolve the spatial and spectral information on the light emission simultaneously.[14] With this system, we observe SP radiation from nanoscale gratings, enabling a drastic reduction of the electron beam energies, which pushes toward the development of efficient on-chip tunable light sources (illustrated in Figure 1). With the ability to fabricate ever-reducing feature sizes, our work provides a platform to bring SP radiation from accelerator physics and high-energy electron physics to integrated devices. A similar motivation has recently led to reducing the velocity threshold of Cherenkov radiation.[18] The unique prospect opened up by compact new SP sources of light lies in their tunability because their emission wavelength can be controlled by the electron velocity and can reach spectral ranges that conventional light sources cannot commonly achieve. These ranges include the EUV and soft X-ray radiation ranges, with numerous exciting applications.[28,29] So far, SP radiation has yet to be experimentally demonstrated in these regimes, even though there have been promising advances toward the realization of an efficient SP source in the UV regime.[30,31]

METHODS

Fabrication. SP gratings were fabricated on Au-coated Si substrates. An Au coating layer was deposited by electron-beam evaporation of 5 nm of Ti and then 200 nm of Au onto a Si chip. A ∼70 nm film of poly(methyl methacrylate) (PMMA) was spin-coated onto the Au-coated Si chip and then soft-baked at 180 °C. Grating patterns were produced by an Elionix F-125 electron beam lithography system using an accelerating voltage of 125 keV and beam current of 500 pA. Exposed PMMA was developed in 3:1 isopropyl alcohol (IPA)/methyl isobutyl ketone at 0 °C for 30 s (see ref 32) and then dried with flowing N_2 gas. Deposition of 20 nm of Au was done via electron-beam evaporation. Metal lift-off was performed in *N*-methylpyrrolidone (NMP) at 50 °C for approximately 60 min, during which the sample was gently rinsed with flowing NMP. After lift-off, the sample was rinsed with acetone and IPA. Finally, gentle O_2 plasma washing (50 W, 60 s) was applied to remove residual resist and solvents.

Experimental Setup. The experimental setup used for this experiment is shown in Figure 2. We used a JEOL JSM-6010LA scanning electron microscope that we modified for the experiment. The sample was mounted at a working distance of 300 mm and a minor tilt of 1 ± 0.5° in order to enable the identification of the gratings area. The SEM was operated in spot mode with beam current varying between 50 and 187 nA, and the beam waist was computed to be between 1 and 1.5 μm. These conditions are not optimal for imaging; however, they enable the alignment of free electrons to pass in close

DOI: 10.1021/acsphotonics.8b00743
ACS Photonics 2018, 5, 3513−3518

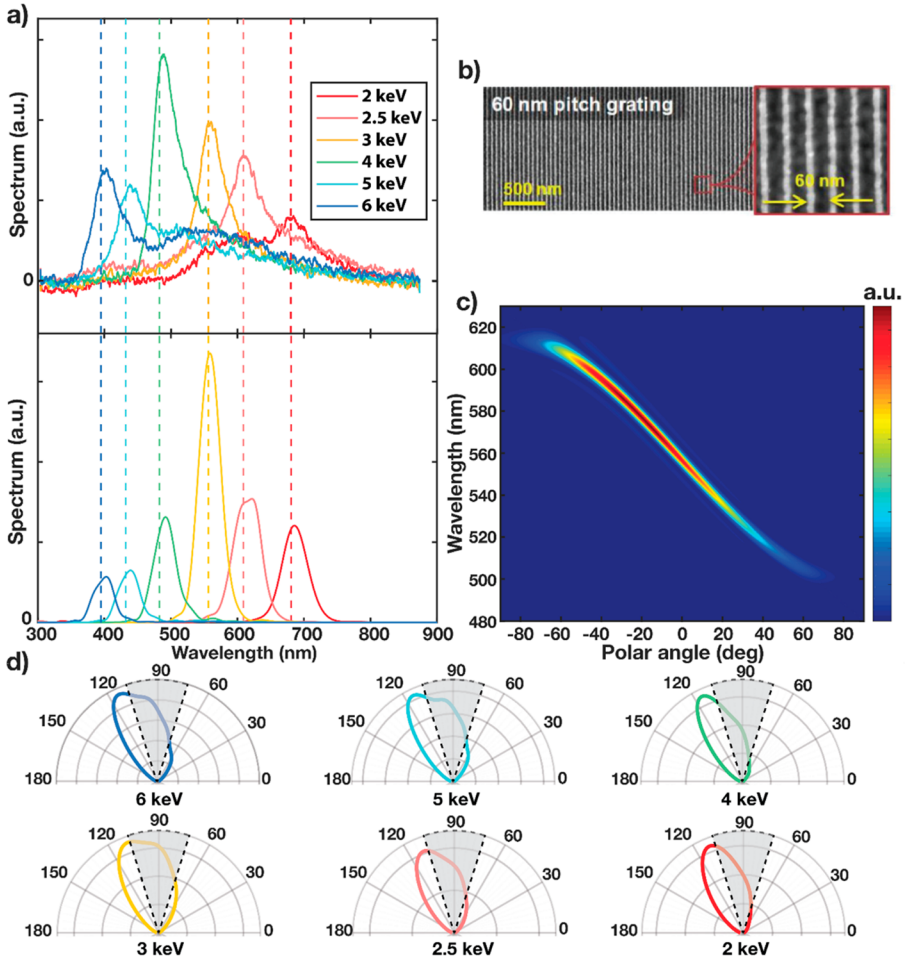

Figure 4. SP radiation from nonrelativistic electrons: measured vs simulated radiation. (a) Upper plot: Measured spectra for different kinetic energies for a 60 nm pitch. Lower plot: Time-domain far-field distribution computed with $N = 20$ unit cells (estimated number of unit cells with which each electron in the beam interacts) and integration over an angle corresponding to the numerical aperture of the objective used in our experiment (NA = 0.3). Differences in relative peak heights result from operating with slightly different currents at different kinetic energies. The dashed vertical lines are calculated according to the conventional SP theory at normal emission,[9] with the same color corresponding to the same kinetic energies. (b) SEM images of 60 nm pitch gratings (the red square shows a zoomed-in display). (c) Simulated angular distribution for a kinetic energy of 3 keV and a grating of $N = 100$ unit cells. The polar angle is measured from the direction normal to the beam propagation. (d) Angular distribution of the SP emission of the same setup as in (c). The shaded gray area corresponds to the numerical aperture of the objective used in our experimental setup.

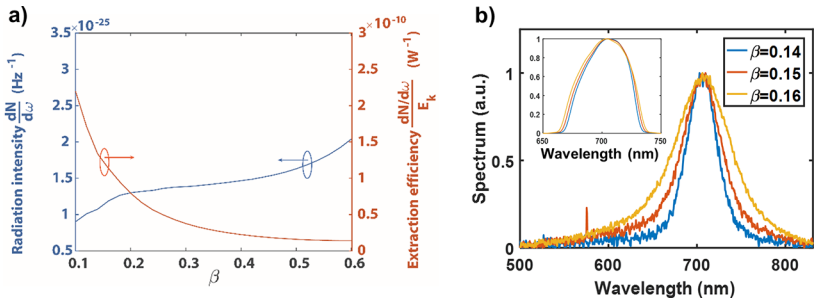

Figure 5. Characterization of SP radiation for slow electrons. (a) Simulated efficiency as a function of β with $\lambda = L/\beta$ fixed at 700 nm. The blue curve represents the radiation intensity, i.e., the total number of photons/Hz/period/electron measured at a fixed wavelength of 700 nm. The red curve represents the extraction efficiency of the SP emission defined as the ratio of the emitted photon energy to the kinetic energy of the incident electron. (b) Normalized measured and simulated (inset) radiated spectra for various β, showing an increase of spectral coherence (bandwidth reduction).

proximity to the surface of the periodic structures. The emitted light was collected with a Nikon TU Plan Fluor 10× microscope objective with a numerical aperture (NA) of 0.30. The emitted SP photons exited the SEM chamber via a leaded glass window and were detected with a spectrometer (Acton SP-2360) equipped with a low-noise thermoelectrically cooled CCD (Princeton Instrument PIXIS-400B). The spectra were collected using a grating with a line density of 150 g/mm

DOI: 10.1021/acsphotonics.8b00743
ACS Photonics 2018, 5, 3513−3518

and a blaze angle of 500 nm while using a low-noise ADC at the rate of 100 kHz. The exposure time was 600 ms, and the signals were averaged over 20 repetitions. Since the beam is focused on the sample at a grazing angle, a significant portion of the beam strikes on the sample and gives rise to an incoherent cathodoluminescence background. We recognize the characteristic SP radiation peaks by subtracting from the total intensity the signal obtained when the beam is located on the sample and away from the grating area. After each measurement set, the stage is moved so the sample is far from the electron path, and the electrons are free to hit the Faraday cup. The electron beam currents were measured using a Keithley 6485 picoammeter.

Calibration. To estimate the absolute emitted optical power of the SP radiation, we performed a power calibration measurement. Using the same experimental configuration of the SP measurements, a calibrated source (AvaLight-HAL-CAL) for the visible range (350−1095 nm) was placed at the same location as the sample. The signal measure for the calibrated light source was obtained at the spectrometer in units of signal counts. The power calibration profile was obtained by measuring the calibrated source using an optical spectrum analyzer (AQ-6315A). The experimental setup response function was obtained by dividing the measured profile of the calibration source by its calibration profile. The SP spectral power from a sample was then obtained by dividing the measured signal from the sample by the setup response function.

Time and Frequency Domain Representation of the Electron Beam. The electron beam can be represented as a time-dependent propagating point electron: $J(\vec{r}, t) = -ev\,\delta(x - vt)\,\delta(y - y_0)\,\delta(z - z_0)\,\vec{x}$, where e is the electron charge. Taking the Fourier transform of this time-dependent distribution, we get the following frequency-domain representation and the associated polarization distribution: $J(\vec{r}, \omega) = -e\exp\left(-i\frac{\omega x}{v}\right)\delta(y - y_0)\,\delta(z - z_0)\vec{x}$ and $P(\vec{r}, \omega) = i\frac{e}{\omega}\exp\left(-i\frac{\omega x}{v}\right)\delta(y - y_0)\,\delta(z - z_0)\vec{x}$. In time-domain simulations, we can use a set of closely spaced dipole sources to mimic the propagation of the electron beam and compare these results with frequency-domain simulations, where we can directly implement a line current.

Time-Domain Simulations. The correspondence between current and polarization distributions allows us to represent an electron beam as a set of closely spaced dipoles shifted in time. Time-domain simulations were run using the commercial FDTD software (Lumerical), where a dipole in frequency domain is defined by its source norm $s(\omega)$ and base amplitude p_{base} as $p_k(\omega, \vec{r}) = p_{\text{base}}s(\omega)\exp\left(-\frac{i\omega x_k}{v}\right)$, where x_k is the position of the kth dipole and the exponential term in the frequency domain corresponds to a time delay in the time domain. The induced polarization by the set of dipoles will be $\sum_{i=1}^{N_{\text{dip}}} p_k(\omega, r) \xrightarrow{N_{\text{dip}} \to +\infty} P(\vec{r}, \omega)$. To ensure that the field recorded is generated by the emission of one electron of charge e, we normalized the recorded electric field by α and power by α^2, where $\alpha = \frac{e\Delta x}{p_{\text{base}}s(\omega)\omega}$.

We usually measure the power on a plane and get a result $P(\omega)$ in units of $\frac{\text{W}}{\text{Hz}^2}/\text{m}^2$. Integrating this result on a surface already simplifies the units to W/Hz^2. This result can be converted into number of photons (per electron): $N_{\text{SP}} = \int \frac{P(\omega)}{\hbar\omega}\text{d}\omega$.

In Figure 4a, simulation parameters are designed to match the results from our experimental setup. For a mean tilt angle of the electron beam of $1 \pm 0.5°$, a pitch of 60 nm, and assuming the electron beam effectively interacts with the grating at a distance $H < 5$ nm (since the interaction efficiency drops exponentially with the pitch as $e^{-4\pi H/a}$), we get an effective number of unit cells of $N \leq 20$. The field is recorded 1 μm above the grating and projected into the farfield. Only radiation emitted at an angle less than the numerical aperture of the objective used in the experiment contributes to the spectrum plotted in Figure 4a. In Figure 4d, a simulation setup similar to that in Figure 4a is used to measure the angular pattern of the radiation.

The simulation setup used to fit the power estimates from our experiment uses the number of unit cells as a fitting parameter and is described in the Supporting Information.

Frequency Domain Simulations. Figure 5a was obtained using the finite-element method (COMSOL Multiphysics). Electrons are treated as a line current (see the Fourier transform in the time-domain simulation) with periodic boundary condition imposed.

Power Estimation. Modeling the entirety of the complex phenomenon of the electron beam hitting a finite number of unit cells involves several challenges: for low-energy electrons, the beam diameter and angular spread increase and depend on many empirical parameters that cannot be estimated in our current experimental setup. Moreover, current theories neglect the divergence effect in the limit where the electron is arbitrarily close to the grating, and a numerical simulation for very short distance would result in arbitrary dependence on the mesh size. To match our experimental power estimate, we use a simplified model of electrons passing at a constant height and use the number of unit cells (or, equivalently, the angle between the beam and the horizontal direction) as a fitting parameter. The measured angle increases for low kinetic energies, as one would except for a wider angular beam spread.

■ ASSOCIATED CONTENT

Supporting Information

The Supporting Information is available free of charge on the ACS Publications website at DOI: 10.1021/acsphotonics.8b00743.

Additional information (PDF)

■ AUTHOR INFORMATION

Corresponding Author

*E-mail: aviram@mit.edu.

ORCID

Aviram Massuda: 0000-0002-0451-1321

Yi Yang: 0000-0003-2879-4968

Author Contributions

I.K. and M.S. conceived the project. Yujia Y. and A.M. fabricated and prepared the samples under study. A.M., C.R.-C., S.E.K., and C.M. performed the experiment. Yi Y. and C.R.-C. performed the numerical simulations. K.K.B., I.K., and M.S. supervised the project. A.M. wrote the manuscript with input from all authors.

Notes

The authors declare no competing financial interest.

DOI: 10.1021/acsphotonics.8b00743
ACS Photonics 2018, 5, 3513−3518

■ ACKNOWLEDGMENTS

The authors would like to thank Dr. Richard Hobbs, Dr. Philip Keathley, Dr. William Putnam, and Dr. Chung-Soo Kim for useful discussions and Kangpeng Wang and Justin Beroz for providing us with Figures [1,] and Figure [2]. We also thank Mark Mondol and Jim Daley for assistance with fabrication and Dr. Peter Krogen for assistance with the experimental setup. We are grateful to Pamela Siska and Susan Spilecki for critical reading and editing of the manuscript. The work was supported by the Army Research Office through the Institute for Soldier Nanotechnologies under contract no. W911NF-18-2-0048 and W911NF-13-D-0001. We thank Kam Chow and Nancy Luy (Lumerical Inc.) for useful advice in setting up time-domain simulations. Yi Yang was partly supported by the MRSEC program of the National Science Foundation under grant no. DMR-1419807. The research of I. Kaminer was partially supported by the Seventh Framework Programme of the European Research Council (EP7-Marie Curie IOF) under grant no. 328853-MC-BSiCS. K. K. Berggren and Y. Yang would like to acknowledge generous support of this research by Arthur Chu and Jariya Wanapun.

■ REFERENCES

(1) Neo, Y.; Shimawaki, H.; Matsumoto, T.; Mimura, H. Smith-Purcell radiation from ultraviolet to infrared using a Si field emitter. *J. Vac. Sci. Technol. B* **2006**, *24* (2), 924−926.

(2) Adamo, G.; MacDonald, K. F.; Fu, Y. H.; Wang, C. M.; Tsai, D. P.; García de Abajo, F. J.; et al. Light Well: A Tunable Free-Electron Light Source on a Chip. *Phys. Rev. Lett.* **2009**, *103* (11), 113901.

(3) Peralta, E. A.; Soong, K.; England, R. J.; Colby, E. R.; Wu, Z.; Montazeri, B.; et al. Demonstration of electron acceleration in a laser-driven dielectric microstructure. *Nature* **2013**, *503* (7474), 91−94.

(4) Li, G.; Clarke, B. P.; So, J.-K.; MacDonald, K. F.; Zheludev, N. I. Holographic free-electron light source. *Nat. Commun.* **2016**, *7*, 13705.

(5) Wong, L. J.; Kaminer, I.; Ilic, O.; Joannopoulos, J. D.; Soljačić, M. Towards graphene plasmon-based free-electron infrared to X-ray sources. *Nat. Photonics* **2016**, *10* (1), 46−52.

(6) Schächter, L. *Beam-Wave Interaction in Periodic and Quasi-Periodic Structures*; Springer Berlin Heidelberg, 2013.

(7) Hitchcock, A. P. Soft X-ray spectromicroscopy and ptychography. *J. Electron Spectrosc. Relat. Phenom.* **2015**, *200*, 49−63.

(8) Friedman, A.; Gover, A.; Kurizki, G.; Ruschin, S.; Yariv, A. Spontaneous and stimulated emission from quasifree electrons. *Rev. Mod. Phys.* **1988**, *60* (2), 471−535.

(9) Smith, S. J.; Purcell, E. M. Visible Light from Localized Surface Charges Moving across a Grating. *Phys. Rev.* **1953**, *92* (4), 1069−1069.

(10) Salisbury, W. W. Generation of Light from Free Electrons. *Science* **1966**, *154* (3747), 386−388.

(11) Bachheimer, J. P. Experimental Investigation of the Interaction Radiation of a Moving Electron with a Metallic Grating: The Smith-Purcell Effect. *Phys. Rev. B* **1972**, *6* (8), 2985−2994.

(12) Ishizuka, H.; Kawamura, Y.; Yokoo, K.; Shimawaki, H.; Hosono, A. Smith−Purcell experiment utilizing a field-emitter array cathode: measurements of radiation. *Nucl. Instrum. Methods Phys. Res., Sect. A* **2001**, *475* (1−3), 593−598.

(13) So, J.-K.; García de Abajo, F. J.; MacDonald, K. F.; Zheludev, N. I. Amplification of the Evanescent Field of Free Electrons. *ACS Photonics* **2015**, *2* (9), 1236−1240.

(14) Kaminer, I.; Kooi, S. E.; Shiloh, R.; Zhen, B.; Shen, Y.; López, J. J.; et al. Spectrally and Spatially Resolved Smith-Purcell Radiation in Plasmonic Crystals with Short-Range Disorder. *Phys. Rev. X* **2017**, *7* (1), 011003.

(15) Wang, Z.; Yao, K.; Chen, M.; Chen, H.; Liu, Y. Manipulating Smith-Purcell Emission with Babinet Metasurfaces. *Phys. Rev. Lett.* **2016**, *117* (15), 157401.

(16) Remez, R.; Shapira, N.; Roques-Carmes, C.; Tirole, R.; Yang, Y.; Lereah, Y.; et al. Spectral and spatial shaping of Smith-Purcell radiation. *Phys. Rev. A: At., Mol., Opt. Phys.* **2017**, *96* (6), 061801.

(17) García de Abajo, F. J. Optical excitations in electron microscopy. *Rev. Mod. Phys.* **2010**, *82* (1), 209−275.

(18) Liu, F.; Xiao, L.; Ye, Y.; Wang, M.; Cui, K.; Feng, X.; et al. Integrated Cherenkov radiation emitter eliminating the electron velocity threshold. *Nat. Photonics* **2017**, *11*, 289.

(19) Tsesses, S.; Bartal, G.; Kaminer, I. Light generation via quantum interaction of electrons with periodic nanostructures. *Phys. Rev. A: At., Mol., Opt. Phys.* **2017**, *95* (1), 013832.

(20) Shaffer, T. M.; Pratt, E. C.; Grimm, J. Utilizing the power of Cerenkov light with nanotechnology. *Nat. Nanotechnol.* **2017**, *12* (2), 106−117.

(21) Schmitz, C.; Wilson, D.; Rudolf, D.; Wiemann, C.; Plucinski, L.; Riess, S.; et al. Compact extreme ultraviolet source for laboratory-based photoemission spectromicroscopy. *Appl. Phys. Lett.* **2016**, *108* (23), 234101.

(22) Kauffman, R. L.; Phillion, D. W.; Spitzer, R. C. X-ray production ~ 13 nm from laser-produced plasmas for projection x-ray lithography applications. *Appl. Opt.* **1993**, *32* (34), 6897−6900.

(23) Goldstein, M.; Walsh, J. E.; Kimmitt, M. F.; Urata, J.; Platt, C. L. Demonstration of a micro far-infrared Smith−Purcell emitter. *Appl. Phys. Lett.* **1997**, *71* (4), 452−454.

(24) Wortman, D. E.; Leavitt, R. P.; Dropkin, H.; Morrison, C. A. Generation of millimeter-wave radiation by means of a Smith-Purcell free-electron laser. *Phys. Rev. A: At., Mol., Opt. Phys.* **1981**, *24* (2), 1150−1153.

(25) Korbly, S. E.; Kesar, A. S.; Sirigiri, J. R.; Temkin, R. J. Observation of Frequency-Locked Coherent Terahertz Smith-Purcell Radiation. *Phys. Rev. Lett.* **2005**, *94* (5), 054803.

(26) Liu, W.; Lu, Y.; Wang, L.; Jia, Q. A multimode terahertz-Orotron with the special Smith−Purcell radiation. *Appl. Phys. Lett.* **2016**, *108* (18), 183510.

(27) Clarke, B. P., So, J., MacDonald, K. F., Zheludev, N. I. Smith-Purcell Radiation from Compound Blazed Gratings. *arXiv preprint arXiv:171109018*, **2017**.

(28) Ackermann, W.; Asova, G.; Ayvazyan, V.; Azima, A.; Baboi, N.; Bähr, J.; et al. Operation of a free-electron laser from the extreme ultraviolet to the water window. *Nat. Photonics* **2007**, *1*, 336.

(29) Sakdinawat, A.; Attwood, D. Nanoscale X-ray imaging. *Nat. Photonics* **2010**, *4* (12), 840−848.

(30) García de Abajo, F. J. Interaction of Radiation and Fast Electrons with Clusters of Dielectrics: A Multiple Scattering Approach. *Phys. Rev. Lett.* **1999**, *82* (13), 2776−2779.

(31) Yang, Y., Massuda, A., Roques-Carmes, C., Kooi, S. E., Christensen, T., Joannopoulos, J. D., et al. Maximal spontaneous photon emission and energy loss from free electrons. *Nat. Phys.*. **2018**, DOI: 10.1038/s41567-018-0180-2.

(32) Cord, B.; Lutkenhaus, J.; Berggren, K. K. Optimal temperature for development of poly(methylmethacrylate). *J. Vac Sci. Technol, B* **2007**, *25* (6), 2013−2016.

■ NOTE ADDED AFTER ASAP PUBLICATION

This paper was published on the Web on September 4, 2018, with errors in Figure 5, panel a. The corrected version was reposted on September 5, 2018.

DOI: 10.1021/acsphotonics.8b00743
ACS Photonics 2018, 5, 3513−3518